JOURNAL OF THERMOPHYSICS AND HEAT TRANSFER
Vol. 8, No. 2, April–June 1994

Conjugate Conduction-Convection Heat Transfer with a High-Speed Boundary Layer

Frederick L. Shope*
Arnold Engineering Development Center, Arnold Air Force Base, Tennessee 37389

A space-marching boundary-layer program has been extensively modified to model conjugate conduction-convection heat transfer for the case of coflowing high-speed gas and liquid coolant. Solid body conduction is modeled as one-dimensional, constant property heat transfer. The coolant is modeled empirically as a bulk fluid with combined forced convection and subcooled nucleate boiling. The flow solver was modified to solve the group of conjugate boundary equations simultaneously and implicitly with the existing momentum and energy equations for the gas. The resulting conjugate conduction-convection program has been applied to analysis of failure of a backside water-cooled nozzle for a high enthalpy, supersonic wind tunnel. The computational results have been used to establish that the primary failure mode is nucleate-boiling burnout and to propose a numerical burnout limit applicable to the specific nozzle configuration.

Nomenclature

C_{nb} = calibration constant in the nucleate-boiling model
C_p = specific heat
D_h = hydraulic diameter; for an annulus, $2(R_{w-1} - R_{w0})$
g = acceleration of gravity
H_{gj} = total enthalpy of the gas at radial station j, $j = 1, 2$ (see Fig. 1)
H_{lv} = latent heat of vaporization of the coolant
h = heat-transfer coefficient
k = thermal conductivity
m_c = mass flow rate of the coolant
Nu_{Dh} = forced convection Nusselt number based on hydraulic diameter
Pr = Prandtl number
q_1 = heat flux on the gas-side of the wall
R_{wj} = wall radius at radial station j, $j = -1, 0, 1$ (see Fig. 1)
Re_{Dh} = Reynolds number based on hydraulic diameter
T = temperature
W = weighting factor for computing the heat transfer at the midpoint of the marching increment, nominally 0.5; see Eqs. (6) and (12)
W_c = weighting factor for averaging results of successive fixed point iterations, nominally 0.9; see Eq. (13)
δA = heat-transfer surface area of a conical frustum at the interface between the wall and the gas, and spanning one computational marching increment
δY = gas-side grid spacing at the wall
θ = slope angle of the air-side wall
μ_c = dynamic viscosity of the coolant
ρ = density
σ = surface tension of the coolant at the saturation temperature for the nucleate-boiling model

Subscripts
c = coolant
fc = forced convection
g = gas
j = radial station, $-1, 0, 1, 2$ (see Fig. 1)
l = saturated liquid
nb = nucleate boiling
v = saturated vapor
w = wall

Superscripts
n = marching station
v = fixed-point iteration counter

Introduction

THE analysis of structures subject to aerodynamic heating and active cooling requires simultaneous consideration of heat transfer through a gas film, within the structure, and to the coolant. Most existing computational fluid dynamics (CFD) and heat conduction codes require that either the wall temperature or the wall heat flux be specified as a boundary condition. Both of these are unknown without a complete simultaneous analysis of the heat-transfer problem within the gas, solid, and coolant.

The literature is replete with reports of analyses of conjugate heat-transfer problems, and a comprehensive review is not attempted here. It is now common to encounter solutions of two-dimensional fluid flow coupled to two-dimensional heat conduction. Compressibility is often admitted, though typically only via a Boussinesq equation of state (density a function only of temperature). Correspondingly, the flow regime has usually been limited to low speed.

A variety of solution procedures has been reported for conjugate heat transfer. Forced convection on a flat plate[1] and a jet impinging on a plate[2] have been solved with analytical methods, but most approaches involve numerical techniques. Some approaches are a limited extension of an existing CFD technique where the conduction problem is treated via a more complex boundary condition.[3] Some methods[4,5] treat the conduction and convection regions with equal emphasis, but employ an analytical transformation to reduce the number of dimensions requiring numerical integration. The next level

Presented as Paper 91-5033 at the AIAA 3rd International Aerospace Planes Conference, Orlando, FL, Dec. 3–5, 1991; received March 16, 1993; revision received Sept. 29, 1993; accepted for publication Oct. 1, 1993.

*Principal Engineer, Calspan Corporation/AEDC Operations, Computational Fluid Dynamics Section, 740 Fourth St. Senior Member AIAA.

of increased complexity is to solve each region separately with a full numerical method, iterating between the two solutions until convergence is attained.[6-8] Finally, the state of the art at present is represented by a close-coupled, fully implicit numerical solution of the entire set of convection and conduction equations.[9-12]

The method of this article is not precisely under any one of the above suggested categories. Here, an existing method is used which solves each of the conservation equations for the gas separately, as conventional, nonblocked, tridiagonal systems of the form $Ax = b$. To solve the solid conduction, coolant convection, and the coolant energy equations, the matrix A and the vectors x and b are enlarged to admit three additional equations and variables.

In particular, a space-marching boundary-layer program, due originally to Patankar and Spalding,[13] has been extensively modified to model conjugate conduction-convection heat transfer for the case of coflowing gas and coolant. Solid body conduction is modeled as one-dimensional (conical), constant property heat transfer. The coolant is modeled as a bulk fluid with combined forced convection and nucleate boiling. The forced convection model for the coolant is for turbulent flow in an annulus; and the nucleate-boiling model is for subcooled pool boiling, i.e., boiling in a nonflowing fluid with its bulk temperature below saturation. The Patankar-Spalding flow solver, which is an implicit decoupled finite difference solution of the momentum and energy equations in von Mises coordinates, was modified to solve the group of boundary equations simultaneously with the existing momentum and energy equations for the gas. Because nucleate boiling is such a highly nonlinear phenomenon (heat transfer is proportional to the cube of the driving temperature difference), the flow solver was further modified from the original noniterative implicit procedure to an iterative implicit procedure. The code has been applied to analysis of a backside water-cooled nozzle for a high enthalpy wind tunnel to assess the cause of catastrophic failures.

This article gives the mathematical model for the conduction-convection boundary conditions, discusses the modified flow solver, and presents computational results and validation data for a water-cooled nozzle used with an arc-heated wind tunnel.

Physical Description

The idealized physical situation modeled herein is illustrated in Fig. 1. A steady, high-temperature, high-speed gas boundary layer flows over a relatively flat surface, in the present application—a contoured nozzle. Outside of the boundary layer, the inviscid gas flow is generally nonuniform and has a decreasing total temperature approaching the wall. In the present model, the gas is assumed to be ideal with constant specific heats. An effective specific heat ratio—chosen to yield the equilibrium Mach number at the specified exit-to-throat area ratio—has been found to yield acceptable engineering accuracy for nozzle exit Mach numbers below about 3 (an equilibrium thermodynamic model would be preferable). Transport properties for the gas are functions of temperature. Radiation heating of the surface by the high-temperature gas has been found to be insignificant (based on analyses not reported here). The boundary layer is axisymmetric and is sufficiently thin so that it does not interact strongly with the inviscid flow. In the contraction region, the boundary-layer thickness decreases markedly approaching the throat as the mass *flux* reaches a maximum at the sonic point. The increase in mass flux requires less flow area for a given mass flow rate and generally overwhelms the tendency of the boundary layer to entrain additional fluid in the contraction; thus, the boundary layer thins. Commensurate with the variation of boundary-layer thickness, the gas-side heat flux and wall temperature reach peaks near the throat. The peaks typically occur slightly upstream of the geometric throat because of the curved sonic line. The boundary-layer flow is turbulent, and the edge temperature is much larger (by about a factor of 5) than the wall temperature. Thus, there is significant convection heat transfer to the wall from the gas, and survival is of concern. The solid wall is thin relative to its length, and conduction in the streamwise direction is small compared to that in the radial direction. The thermal properties of the wall material are approximately constant. The solid wall is cooled with a liquid flowing in the same direction as the gas. The wall temperature at radial station $j = 0$ (see Fig. 1) may be greater than the saturation temperature of the liquid coolant. The coolant passage height is similar to the wall thickness, and the coolant flow is turbulent and fully developed. The coolant receives heat from the wall via turbulent forced convection enhanced by nucleate boiling. The coolant remains significantly below its saturation temperature, and the boiling regime may be regarded as subcooled boiling. The coolant passage wall at station $j = -1$ (Fig. 1) is assumed to be at the local bulk fluid temperature and is, therefore, an adiabatic boundary, but is not specifically modeled herein. The specific application is a low Mach number (1.8) supersonic nozzle.

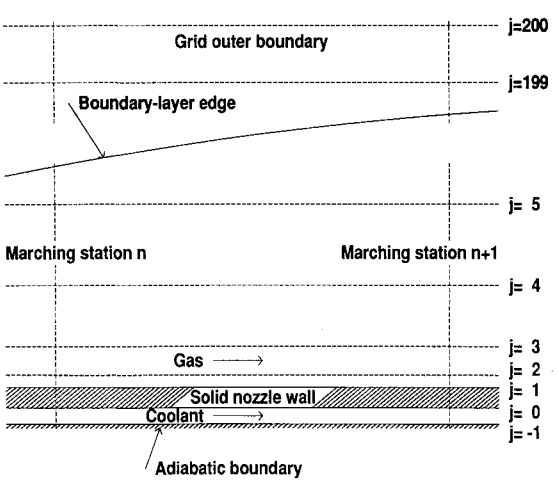

Fig. 1 Notation and flow geometry in boundary-layer coordinates.

Mathematical Model

Existing Boundary-Layer Method

The present method is based on a modification of the Patankar-Spalding boundary-layer program,[13] the present starting point being the version described by Mayne and Dyer.[14] In this method the steady, axisymmetric, compressible boundary-layer equations for conservation of momentum and energy are solved in a streamline (normalized von Mises) coordinate system. The partial differential equations are discretized with a Crank-Nicholson difference scheme. The two parabolic conservation equations are solved in an implicit but decoupled space-marching fashion with a specialized tridiagonal solver. The existing solver is specialized in the sense that the difference equation is assumed to be of the following form:

$$A_i F_{i+1} - F_i + B_i F_{i-1} + C_i = 0 \qquad (1)$$

Here, F is the vector of unknowns, either velocity or total enthalpy; A, B, and C are the constants of the linear system; and the coefficient of F_i is assumed to be 1. The primary unknown dependent variables are velocity and total enthalpy. The operational version of the code includes a Prandtl mixing length turbulence model with van Driest damping near the wall. Boundary-layer edge conditions, which are typically taken from an Euler solution, require specification of edge static and stagnation pressure. Initial velocity and total enthalpy profiles are based on a turbulent power-law profile.

For the present application of flow in an axisymmetric nozzle, the edge conditions have been computed using a time-dependent Euler code.[15]

Conjugate Conduction-Convection Boundary Model

In the following development, the collection of equations comprising the model of the heat-transfer process will be referred to as the boundary model. The boundary model is composed of four parts: 1) heat convection through the gas to the wall, 2) solid-body conduction through the wall, 3) convection from the coolant-side wall to the coolant, and 4) an energy equation for the coolant.

Referring to Fig. 1, the gas-side heat transfer is computed with the one-dimensional Fourier equation with the surface-normal derivative represented by a two-point difference scheme:

$$q_1^{n+1} = k_g(H_{g2}^{n+1} - H_{g1}^{n+1})/(C_{pg}\delta Y) \tag{2}$$

This assumes an ideal gas with constant specific heats and a laminar sublayer at the wall. Thermal conductivity k_g is evaluated at the wall temperature. Note that this *entire* equation is evaluated at marching station $n+1$. H_{g1} and H_{g2} are the total enthalpy at the wall and the first gas-flow station above the wall, respectively. These are primary solution variables in the existing boundary-layer code, and this equation provides the link between the existing code and the new boundary model. In using total enthalpy to compute static temperature gradient, it is assumed that the contribution of kinetic energy is negligible (the velocity is negligible at radial station 2). An axisymmetric version of Eq. (2) is not necessary since $\delta Y \ll R_{w1}$. Enthalpy at the wall is converted to temperature with the usual definition:

$$H_{g1}^{n+1} = C_{pg}T_{w1}^{n+1} \tag{3}$$

Heat transfer through the solid wall is assumed to be conical and one-dimensional in the surface-normal direction:

$$q_1^{n+1} = k_w \cos\theta(T_{w1}^{n+1} - T_{w0}^{n+1})/[R_{w1} \ln (R_{w0}/R_{w1})] \tag{4}$$

Practical experience has shown that in a thin-walled vessel, heat conduction in other than the surface-normal direction is usually negligible. Heat transfer from the wall to the coolant is modeled with a heat-transfer coefficient and a driving temperature difference between the wall and the coolant bulk temperature:

$$R_{w1}q_1^{n+1}/R_{w0} = h_c(T_{w0}^{n+1} - T_c^{n+1}) \tag{5}$$

The heat-transfer coefficient h_c will be modeled below in terms of a forced convection component and a nucleate-boiling component. In Eqs. (2–5), all variables are evaluated at the marching station $n+1$. Finally, an energy equation for the coolant is formed for a simple one-dimensional bulk flow. To preserve second-order accuracy, the heat flux is evaluated at the midpoint of the interval between station n and $n+1$ using a weighted average:

$$m_cC_{pc}(T_c^{n+1} - T_c^n) = \delta AR_{w1}[(1-W)q_1^n + Wq_1^{n+1}]/R_{w0} \tag{6}$$

The coolant specific heat is evaluated at T_c^{n+1}. Equations (2–6) comprise the boundary equations for the conjugate conduction-convection heat-transfer problem.

The remaining portion of the boundary model is the definition of the coolant heat-transfer coefficient h_c. The model may be described as subcooled forced-convection nucleate boiling. The forced convection component of the model is that given by Kays and Crawford[16] for turbulent heat transfer in an annulus. This model is tabular and gives a Nusselt number in terms of a hydraulic-diameter Reynolds number, a Prandtl number, and a radius ratio for the annulus. That is

$$Nu_{Dh} = f(Re_{Dh}, Pr, R_{w0}/R_{w-1}) \tag{7}$$

where the Reynolds number, assuming a narrow annulus, is computed from

$$Re_{Dh} \approx m_c/(\mu_c\pi R_{w-1}) \tag{8}$$

and the Prandtl number is $Pr = \mu_cC_{pc}/k_c$. The Nusselt number yields a forced-convection heat-transfer coefficient h_{fc} via the relation $Nu_{Dh} = h_{fc}D_h/k_c$. Properties are evaluated at the bulk temperature of the coolant.

The boiling component of the model is for subcooled nucleate pool boiling due to Rohsenow as described by Kreith[17]:

$$q_{nb} = \left[\frac{g(\rho_{c,l} - \rho_{c,v})}{\sigma}\right]^{1/2}\left[\frac{C_{pc}(T_{w0} - T_{c,l})}{C_{nb}}\right]^3 (Pr_c)^{-m}\frac{\mu_c}{H_{fv}^2} \tag{9}$$

Here, the various coolant properties are evaluated at the saturation temperature (not the bulk temperature) corresponding to the local static pressure of the liquid coolant. For the present effort, tabular models for water have been employed from Refs. 17 and 18. The empirical constant C_{nb} ($=0.027$ here) varies with the type of wall material; and the exponent m ($=3$ here) depends on the type of coolant. The value $C_{nb} = 0.027$ is based on the data of Schaefer and Jack.[19] This model is for pool boiling, that is, boiling in a nonflowing fluid. It may be deficient for the present application in that it does not depend upon flow parameters such as velocity, except indirectly via the saturation pressure. However, at present there are no known alternatives. A test facility and experiment with nucleate boiling in flowing water are under development at AEDC to characterize the heat transfer for the present parameter range of interest.

In modeling flow with boiling, a heuristic but suitable modeling approach is to assume that the total heat transfer is the sum of contributions from forced convection and nucleate boiling.[17] Consistent with the industry custom of using heat-transfer coefficients and driving temperature differences, the present model is

$$h_c = h_{fc} + h_{nb} \tag{10}$$

where

$$h_{nb} = q_{nb}/(T_{w0} - T_c) \tag{11}$$

and h_{fc} is obtained from Eq. (7) and the definition of the Nusselt number, $Nu_{Dh} = h_{fc}D_h/k_c$. Equation (10) provides the tie-in between the primary model equations—particularly through Eq. (5)—and the convection and boiling models.

Many correlations have been advanced for the critical heat flux (the limiting peak on heat transfer beyond which burnout may be expected), but the predictions vary widely, and none has been found to quantitatively model the process of the present application. Thus, the present model does not yet contain a generally applicable burnout criterion; but the nucleate-boiling experiment mentioned above is intended to redress this deficiency.

Implementation of the Conjugate Boundary Model

The boundary model described above was implemented in the Patankar-Spalding boundary-layer program. The existing solver routine is based on a tridiagonal inverter, and it was deemed desirable to implement the boundary model in this way. Equations (2–6) are solved as linear equations which are part of the existing system of difference equations for the energy equation. Thus, the existing coefficient and solution vectors are simply extended to make room for additional equations and variables. The primary solution variables in Eqs. (2–6) are H_{g2}, H_{g1}, q_1, T_{w1}, T_{w0}, and T_c. H_{g1} and H_{g2} were already part of the original variable set. Unfortunately, the new boundary equations are not tridiagonal. To alleviate

this difficulty, Eqs. (5) and (6) and variables T_c and T_{w0} were analytically eliminated from the system. In the analytically reduced boundary system, the final version of Eq. (4) was replaced by

$$-\left(\frac{1}{h_c}+\frac{W\delta A}{m_c C_{pc}}+\frac{R_{w0}}{k_w\cos\theta}\,/\!/\,\frac{R_{w0}}{R_{w1}}\right)q_1^{n+1}+\frac{R_{w0}}{R_{w1}}T_{w1}^{n+1}=\frac{R_{w0}}{R_{w1}}T_c^n+\frac{(1-W)\delta A}{m_c C_{pc}}q_1^n \tag{12}$$

Thus, the final system of boundary equations solved in the computer program is comprised of Eqs. (2), (3), and (12) with unknowns H_{g2}, H_{g1}, q_1, and T_{w1}. This elimination yielded a tridiagonal system, but also resulted in a zero coefficient on the diagonal. The zero precludes use of the original tridiagonal inverter, which assumes that the diagonal coefficient is 1. Hence, a more general tridiagonal inverter from Ref. 20 was inserted in place of the original. Additional details are given in Ref. 21. [Please note present corrections to Eqs. (5), (6), and (12) of Ref. 21.]

Initially, stable marching was not obtained. The instability was dealt with by implementing two remedies: 1) a fixed-point iteration at each station, and 2) a weighted average of successive iterative values of the nucleate-boiling coefficient. The most effective average was found to be

$$h_{nb}^{\nu+1}=\{W_c[\max(h_{nb}^{\nu+1},h_{nb}^{\nu})]^2+(1-W_c)[\min(h_{nb}^{\nu+1},h_{nb}^{\nu})]^2\}^{1/2} \tag{13}$$

where ν is the iteration number at the fixed marching station $n+1$. The weight W_c was found to be important for convergence: a value of 0.9 has consistently yielded reliable results. After an initial transient, the fixed point iteration has been found to converge in less than 20 iterations. The iteration procedure has about doubled the Convex 3840 CPU time, requiring about 50 s for the application described below ($\approx 3.1 \times 10^{-5}$ s/grid point/space step). The final computer code is referred to as the conjugate conduction-convection program (CCCP).

Results

Application

The analysis technique described above was developed as part of an effort to design water-cooled nozzles which can survive in advanced high enthalpy test facilities. One wind-tunnel facility receiving developmental attention is the AEDC 40 MW segmented electric arc-heated high enthalpy ablation test unit (HEAT-H1[22]). In HEAT-H1, air is heated continuously by passing an electric arc through a column of high pressure air 5 cm in diameter and about 2-m long. The heated air is expanded through a water-cooled, contoured, supersonic nozzle designed to provide a region of uniform flow. This facility currently operates routinely at bulk stagnation conditions of 100 atm and 7000 kJ/kg (2.4 kg/s of air at a bulk temperature of about 4500 K). New test requirements, such as propulsion and material testing for aerospace planes, have spurred development of a 200 atm capability at flow rates requiring perhaps 400 MW (nominally 45 kg/s). Initial attempts to operate HEAT-H1 at higher pressure have resulted in nozzle failures above about 130 atm. Thus, a primary application of the present capability is to improve the design of the nozzles for HEAT-H1.

The nozzle configuration, which has been used successfully for many years at AEDC, is the backside water-cooled nozzle shown in Fig. 2. The nozzle material is a copper-zirconium alloy. The nozzle under study has a throat diameter of 2.29 cm (0.9 in.) and is designed for parallel exit flow at Mach number 1.8. The wall thickness is 0.16 cm (0.062 in.) at the throat. The overall length of the continuous nozzle section is 5.8 cm (2.3 in.). The calculations presented herein are for the flow conditions summarized in Table 1. Note that nozzle failure occurred for cases II and IV. Case II was at very high stagnation enthalpy, while case IV was at somewhat lower enthalpy, but at about 60% of the coolant flow rate.

Table 1 Air and water flow conditions for the test cases

	Case number			
	I	II	III	IV
Air total pressure, atm	126.5	137	104.4	94.3
Air total temperature, K	5000	5240	4600	5100
Air total enthalpy, kJ/kg	8094	8722	7122	8476
Air total enthalpy, Btu/lbm	3480	3750	3062	3644
Water mass flow rate, kg/s	5.234	5.234	3.216	3.204
Water mass flow rate, lbm/s	11.54	11.54	7.090	7.063
Water inlet temperature, K	309	307	289	289
Water inlet pressure, atm	68	68	68	68
Water inlet pressure, psia	1000	1000	1000	1000
Water temperature rise, K	13.9	15.0	18.9	20.0
Water temperature rise, °R	25	27	34	36
Survival/failure		Fail		Fail

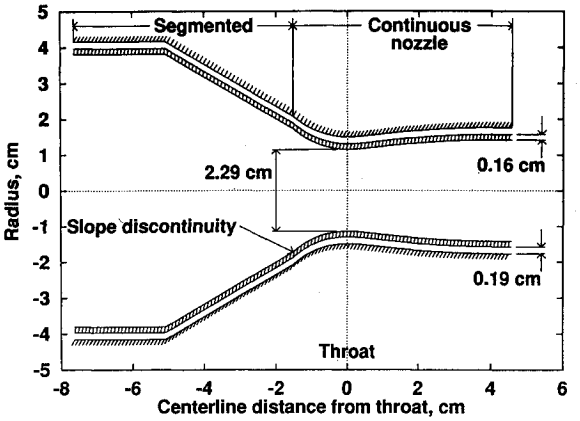

Fig. 2 Nozzle geometry as modeled.

The geometry is modeled here in a somewhat idealized form. The 7.6-cm- (3-in.-) diam section and the conical contraction are composed of arc heater segments with annular depressions between adjacent segments. Hence, the actual air-side surface of the segmented portion has a considerable surface roughness which is not modeled here. Entry length effects of this roughness on the smooth nozzle surface should be diminished by acceleration of the gas in the contraction, which has a laminarizing effect. Also, each segment has its own coolant inlet and outlet. For the present calculations, a continuous annular passage is assumed for the entire length of the device shown in Fig. 2. Note the small slope discontinuity at about the −1.5-cm station.

To initiate the analysis, a time-dependent Euler[15] solution was obtained to define the edge static pressure for the boundary-layer solution. This was an ideal gas solution with specific-heat ratio of 1.24. The Euler solution used a subsonic inflow boundary in the 7.6-cm-diam stilling chamber. The upstream boundary condition was uniform stagnation pressure and temperature and parallel subsonic inflow. The exit was a supersonic outflow boundary. The mesh for the Euler solution used 7 radial points, 97 streamwise points, and about 6000 time steps to reduce the residuals by six orders of magnitude. Doubling the number of radial points altered the surface pressure by less than $\frac{1}{2}$%.

The boundary-layer solution for the gas side was initialized with a $\frac{1}{9}$-power-law (turbulent) profile in the stilling chamber region. An initial boundary-layer thickness of 0.30 cm was assumed. The total temperature nonuniformity outside the boundary layer is accounted for in the boundary-layer solution by specifying an edge total enthalpy based on measured profiles at the nozzle exit. For the present calculations, a ratio

of edge-to-bulk total enthalpy of 0.83 was used. The streamwise marching step size was a constant 0.0030 cm, resulting in 3240 marching stations in the streamwise direction. The surface-normal grid in the gas used 200 grid points. The grid was clustered near the surface with a geometric progression which increased each increment by a factor of 1.035 over the previous increment.

Analysis

The discussion that follows presents the results of the calculations. There are very few data for validation of the present calculations since most instrumentation interferes with the cooling process and jeopardizes survival of the nozzle. Validation of most of the results shown will be limited to comparison with subjective observations of facility behavior and with a single measurement, namely, the measured water temperature rise over the length of the cooling jacket.

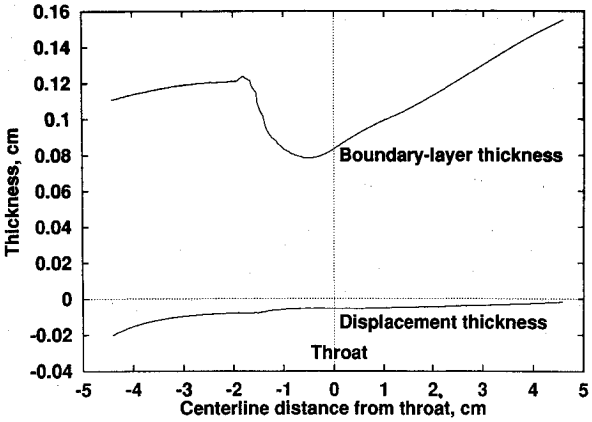

Fig. 3 Boundary-layer and displacement thickness distributions for case I.

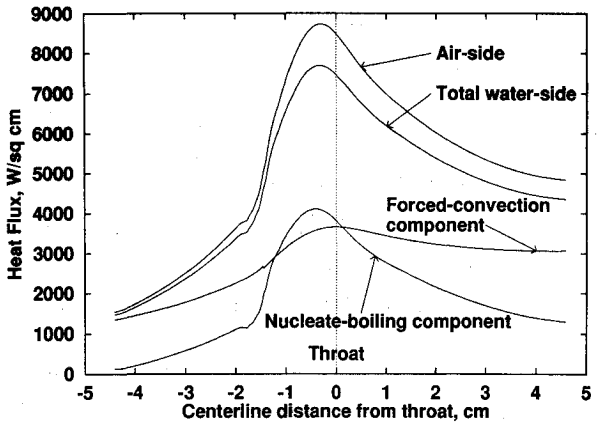

Fig. 4 Heat flux distributions for case I.

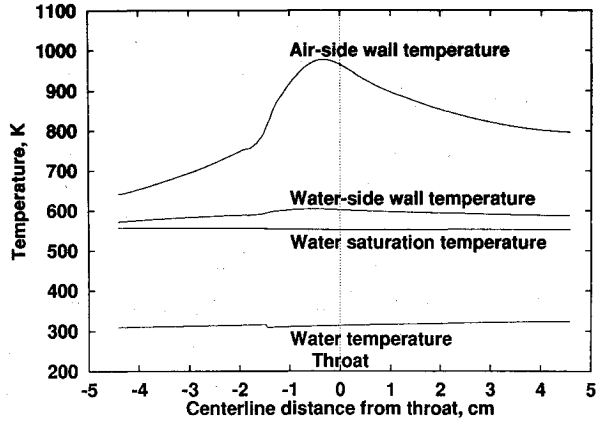

Fig. 5 Temperature distributions for case I.

Figures 3–5 show the results of the computations for case I. Figure 3 shows the distributions of boundary-layer thickness and displacement thickness. The dramatic decrease in boundary-layer thickness in moving toward the throat is associated with the mass flux (mass flow rate per unit area) reaching a peak. The minimum boundary-layer thickness, as expected, occurs slightly upstream of the geometric throat close to where the boundary-layer edge becomes sonic. The small oscillation occurs where the thickness peaks and is associated with the slope discontinuity shown in Fig. 2. The negative displacement thickness is associated with the cold wall. Figure 4 shows the air-side and water-side heat fluxes and the individual contributions to the water-side heat flux by forced convection and nucleate boiling. The water-side heat flux is less than the air-side heat flux because of axisymmetric effects: the water-side surface area is greater than the air-side surface area for a given length of conical frustum. The point of peak heating coincides with the minimum boundary-layer thickness. Notice that the cooling process remains dominated by forced convection over most of the nozzle, except in the peak heating region near the throat. This is consistent with the frequent argument that nucleate boiling turns on and off as needed to handle local peak heat loading. The forced convection peaks at the geometric throat, because the coolant flow area reaches a minimum there and the velocity reaches a maximum. Figure 5 shows the temperature distributions. The slight down step in the water temperature at -1.5 cm results from resetting the otherwise continuous coolant temperature to the measured inlet temperature. This procedure models the actual hardware, where the cooling water is removed from the water jacket just upstream of the nozzle, while the nozzle itself receives a separate, parallel supply from the central manifold. The water temperature rise is small on the scale shown; but even the variation of the water-side wall temperature is relatively small, a well known characteristic of cooling by flow boiling. The small increase in the water-side wall temperature compared to the large increase in boiling heat transfer in Fig. 4 is dramatic evidence of the nonlinearity of boiling effects. In Fig. 5, only the air-side shows large variations, peaking at about 1000 K just upstream of the throat. This large variation is the primary impetus for solving the conjugate heat-transfer problem; otherwise, for a conventional boundary-layer solution, the air-side wall temperature would have to be specified as a boundary condition. The peak temperature is well below the copper-zirconium melt temperature of 1340 K, and the computation predicts that the nozzle will not fail by melting at these conditions. The survival prediction agrees with test facility observation, and this contributes to circumstantial validation of the model. The air-to-water-side temperature gradient is more than an order of magnitude greater than the air-side axial gradient, and the maximum streamwise heat-transfer rate is about 0.6% of the wall-normal heat-transfer rate. This supports the original assumption that streamwise conduction may be neglected. Results comparable to Figs. 3–5 for cases II, III, and IV are qualitatively similar to those shown above and are not presented here.

Figure 6 shows a comparison of the present computations for all four cases with water temperature data from HEAT-H1. Shown here is the ratio of water temperature rise to inlet water temperature in terms of theory vs data. If the computations and data were in exact agreement, the data points would fall precisely on the diagonal. The data points from the four tunnel entries are shown with uncertainty bands of $\pm 7\%$. Considering the range of variation of the parameters and the data uncertainty, the calculations agree reasonably well with the data. The specific water temperature rise is also of interest and is given in Table 2. The calculations differ from the data by at most 1.3 K (8.7%) for case II. Three of the four calculations are within the data uncertainty. The nozzle for case II is believed to have failed before the facility reached

Table 2 Measured and computed water temperature rise

	Case number			
	I	II	III	IV
Measured water temperature rise, K	13.9	15.0	18.9	20.0
Theoretical water temperature rise, K	14.3	16.3	18.0	19.6
Data, +7% uncertainty, K	14.9	16.0	20.2	21.4
Data, −7% uncertainty, K	12.9	14.0	17.6	18.6
Theoretical error, %	2.9	8.7	−4.8	−2.0

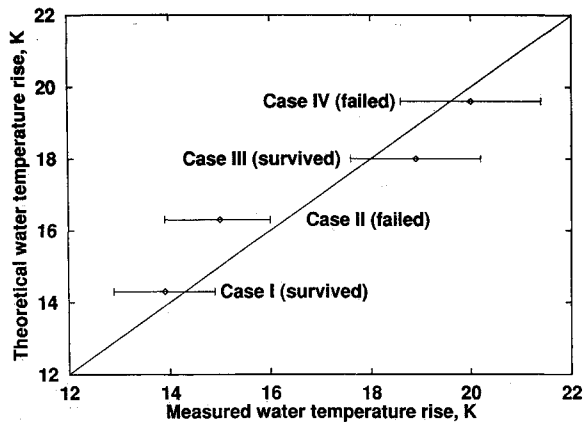

Fig. 6 Comparison of theoretical and measured water temperature rise.

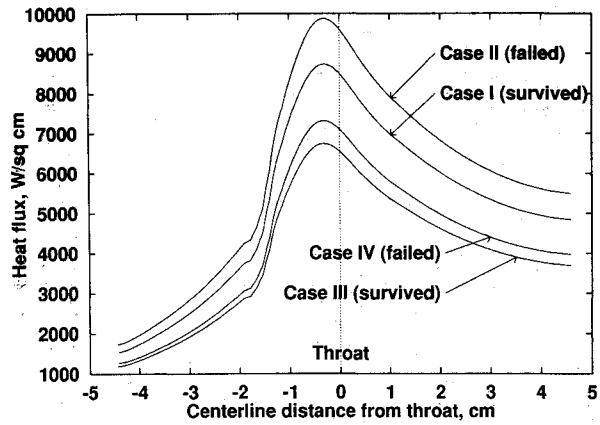

Fig. 7 Comparison of heat-transfer distributions for the four test cases.

steady state, in which case the measured water temperature rise would be less than the steady-state value had the nozzle survived.

As noted in Table 1, cases II and IV resulted in nozzle failures, although the failure mechanism is unknown because the nozzle is completely destroyed in the failure process. The three recognized failure mechanisms are failure by melting, failure due to boiling burnout (heat transfer in excess of the critical heat flux), and conventional stress failure. The theoretical heat-transfer distributions for all four cases are compared in Fig. 7. Note the geometric similarity. Failed case II has the highest peak, but failed case IV lies between surviving cases I and III. The predicted peaks in wall temperature of all four cases are below the melt temperature of the material. Finite element elastic-plastic stress analyses (which admit yield point as a function of temperature) indicate, based on the present heat and pressure loads, that the failures are not due to stress failure. For these reasons, the nozzle failures are believed to be due to nucleate-boiling burnout.

With results from the present calculations, it has been observed that the two nozzle survivals can be segregated from the two failures on the basis of the peak boiling heat flux; i.e., for surviving cases I and III, the peak boiling heat flux is less than that for failing cases II and IV. This result suggests a possible criterion for nucleate-boiling burnout for the present nozzle configuration. That criterion would be that nozzle survival could be expected if the heat flux by nucleate boiling were less than about 4200 W/cm^2. This value is, of course, specific to the present nozzle configuration and the water conditions covered by the data. Further experimental work is required to validate this result and to establish a more general burnout criterion.

Summary and Conclusions

A relatively inexpensive procedure has been advanced for computing the interaction of heat convection in a high-speed boundary layer with heat conduction in a cooled structure. The method couples a boundary-layer solver with a boundary model for the conjugate conduction-convection heat transfer in the structure and coolant. The highly nonlinear effects of nucleate boiling in the coolant have been found to require additional attention, such as iteration at each marching station and weighted averaging of iterates, to achieve stable marching. The method has been applied to evaluation of heating failures in a water-cooled arc tunnel nozzle for which the rise in the temperature of the cooling water has been measured. Reasonably good agreement with limited data suggests that the method is promising. The results of the nozzle analysis suggest that the observed catastrophic failures were due to nucleate-boiling burnout. A failure criterion based on a limiting peak of heat transfer by nucleate boiling has been proposed for the present nozzle configuration.

Acknowledgments

The research reported herein was performed by the Arnold Engineering Development Center (AEDC), Air Force Material Command. Work and analysis for this research were done by personnel of Calspan Corporation/AEDC Operations, technical services contractor for the AEDC aerospace flight dynamics facilities. The author is indebted to Robert C. Bauer, Calspan Corporation/AEDC Operations, who earlier developed (in an unpublished work) a partly empirical and partly analytical engineering mathematical model of the throat cooling process of interest here. The influence of his modeling philosophy on the present effort is significant. In particular, Bauer proposed the idea of a burnout criterion in the form of a limit on boiling heat flux.

References

[1]Pozzi, A., and Lupo, M., "The Coupling of Conduction with Forced Convection over a Flat Plate," *International Journal of Heat and Mass Transfer*, Vol. 32, No. 7, 1989, pp. 1207–1214.

[2]Wang, X. S., Dagan, Z., and Jiji, L. M., "Conjugate Heat Transfer Between a Laminar Impinging Liquid Jet and a Solid Disk," *International Journal of Heat and Mass Transfer*, Vol. 32, No. 11, 1989, pp. 2189–2197.

[3]Maughan, J. R., and Incropera, F. P., "Fully Developed Mixed Convection in a Horizontal Channel Heated Uniformly from Above and Below," *Numerical Heat Transfer*, Pt. A, Vol. 17, No. 4, 1990, pp. 417–430.

[4]Cole, K. D., and Beck, J. V., "Conjugate Heat Transfer from a Hot-Film Probe for Transient Air Flow," *Journal of Heat Transfer*, Vol. 110, No. 2, 1988, pp. 290–296.

[5]Libera, J., and Poulikakos, D., "Parallel-Flow and Counter-Flow Conjugate Convection from a Vertical Insulated Pipe," *Journal of Thermophysics and Heat Transfer*, Vol. 4, No. 3, 1990, pp. 400–404.

[6]Moukalled, F., and Acharya, S., "Forced Convection Heat Transfer in a Finitely Conducting Externally Finned Pipe," *Journal of Heat Transfer*, Vol. 110, No. 3, 1988, pp. 571–576.

[7]Joubert, P., and Le Quere, P., "Numerical Study of Thermal Coupling Between Conductive Walls and a Boussinesq Stratified Fluid," *Numerical Heat Transfer*, Pt. A, Vol. 16, No. 4, 1989, pp. 489–506.

[8]Blank, D. A., "Conjugate Conduction-Convection Heat Transfer Model for the Valve Flow-Field Region of Four-Stroke Piston Engines," *Numerical Heat Transfer*, Pt. A, Vol. 18, No. 3, 1990, pp. 283–308.

[9]Karwe, M. V., and Jaluria, Y., "Fluid Flow and Mixed Convection

Transport from a Moving Plate in Rolling and Extrusion Processes," *Journal of Heat Transfer*, Vol. 110, No. 3, 1988, pp. 655–661.

[10]Lau, S. C., Ong, L. E., and Han, J. C., "Conjugate Heat Transfer in Channels with Internal Longitudinal Fins," *Journal of Thermophysics and Heat Transfer*, Vol. 3, No. 3, 1989, pp. 303–308.

[11]Kuo, J. C., and Lin, T. F., "Steady Conjugate Heat Transfer in Fully Developed Laminar Pipe Flows," *Journal of Thermophysics and Heat Transfer*, Vol. 2, No. 3, 1988, pp. 281–283.

[12]Shaw, H.-J., Chen, C.-K., and Jang, J.-Y., "Natural Convection in an Enclosure Heated from Below with a Conductive Horizontal Partition," *Journal of Thermophysics and Heat Transfer*, Vol. 2, No. 4, 1988, pp. 335–342.

[13]Patankar, S. V., and Spalding, D. B., "A Finite-Difference Procedure for Solving the Equations of the Two-Dimensional Boundary Layer," *International Journal of Heat and Mass Transfer*, Vol. 10, No. 10, 1967, pp. 1389–1411.

[14]Mayne, A. W., and Dyer, D. F., "Comparisons of Theory and Experiment for Turbulent Boundary Layers on Simple Shapes at Hypersonic Conditions," *Proceedings of the 1970 Heat Transfer and Fluid Mechanics Institute*, Monterey, CA, June 1970, pp. 168–188.

[15]Cline, M. C., "NAP: A Computer Program for the Computation of Two-Dimensional, Time-Dependent, Inviscid Nozzle Flow," Los Alamos Scientific Lab., LA-5984, Los Alamos, NM, Jan. 1977.

[16]Kays, W. M., and Crawford, M. E., *Convective Heat and Mass Transfer*, 2nd ed., McGraw-Hill, New York, 1980, pp. 252–256.

[17]Kreith, F., *Principles of Heat Transfer*, 3rd ed., Intertext Press, New York, 1973, pp. 502–515.

[18]Reynolds, W. C., and Perkins, H. C., *Engineering Thermodynamics*, 2nd ed., McGraw-Hill, New York, 1977, pp. 630–633.

[19]Schaefer, J. W., and Jack, J. R., "Investigation of Forced-Convection Nucleate Boiling of Water for Nozzle Cooling at Very High Heat Fluxes," NASA TN D-1214, May 1962.

[20]Anderson, D. A., Tannehill, J. C., and Pletcher, R. H., *Computational Fluid Mechanics and Heat Transfer*, McGraw-Hill, New York, 1984, pp. 549, 550.

[21]Shope, F. L., "Conjugate Conduction/Convection/Nucleate-Boiling Heat Transfer with a High-Speed Boundary Layer," AIAA Paper 91-5033, Dec. 1991.

[22]Horn, D. D., and Smith, R. T., "AEDC High Enthalpy Ablation Test (HEAT) Facility Description, Development, and Calibration," Arnold Engineering Development Center, AEDC-TR-81-10, AD-A101747, Arnold AFB, TN, July 1981.